

## FINITE-ELEMENT MODEL DEVELOPMENT OF SINGLE ASPERITY SCRATCH: A STEP-BY-STEP APPROACH

**K. Pondicherry<sup>1,2</sup>, T. Galle<sup>1</sup>, J. Sukumaran<sup>1</sup>, D. Fauconnier<sup>1</sup>, S. Hertelé<sup>1</sup> and P. De Baets<sup>1</sup>**

<sup>1</sup>*Soete Laboratory, Department of Electrical Energy, Metals, Mechanical Construction and Systems, Ghent University, Technologiepark, Zwijnaarde-903 Ghent, 9052, Belgium  
Tel.: +32 9331 0489, E-mail: kannakishanmugham.pondicherry@ugent.be*

<sup>2</sup>*SIM vzw, Technologiepark 935, BE-9052 Zwijnaarde, Belgium*

*Abstract:* A roadmap and methodology to develop a three-dimensional (3D) finite-element model to simulate single asperity scratch is described in the present study. The step by step evolution from a two-dimensional (2D) static implicit Hertzian line contact model to 3D quasi-static explicit load controlled scratch model is explained. Each step is validated either by analytical models or by experiments. At every step, the model has shown a considerable agreement with the analytical solutions or experimental results. Therefore, scratch depth of metals can be predicted reasonably using the current model. Future work involves an extensive study of the influence of various parameters like indenter geometry, friction, etc.

*Keywords:* Finite-element modelling, 3D scratch model, quasi-static-explicit, Hertzian contact

### INTRODUCTION

A wide variety of research applications such as aerospace, ballistics, welding, fracture and failure analysis, etc. extensively use finite-element modelling as an efficient and effective tool to simulate response of material behaviour under operating conditions of respective fields (Gerbig, Srivastava, Osovski, Hector, & Bower, 2017; Jankowiak, Rusinek, Kpenyigba, & Pesci, 2014; Mason & Warren, 2017; Ni & Abdel Wahab, 2017). Finite-element modelling has also been used to study tribological phenomenon such as wear response of the material and influence of friction (Tobi, Sun, & Shipway, 2017; Yue & Wahab, 2017). Wear is one of the most common causes for component failure in real time applications. Among various types of wear, e.g., erosive, adhesive, fretting; etc., abrasive wear is of significant interest. According to an estimation, abrasive wear is responsible for almost 80-90% of all wear encountered in machine components whereas, fatigue wear follows at far distance with only 8%. Other types of wear are even less common (Zmitrowicz, 2006). Abrasive wear is defined as, wear due to hard particles or hard protuberances forced against and moving along a solid surface (ASTM, 1987). The real system of abrasive wear is too complicated to be simulated using FE modelling. Therefore, a single scratch is the simplest and the most fundamental abstraction of abrasive wear that can be simulated with relatively less hardship.

Scratch indentation has been studied using Finite-Element Modelling (FEM) by many researchers from the perspective of various aspects such as, the influence of indenter geometry, friction coefficient at the contact, dynamic loading conditions etc. (Elwasli, Zemzemi, Mkaddem, Mzali, & Mezlini, 2015; Li & Beres, 2006; Subhash & Zhang, 2002). Many a times, the model development stage lacks a comprehensive description in literature. Hence, in the present work we focus on the methodology and process of model development itself. Therefore, a roadmap and methodology to develop a 3D finite-element model to simulate single asperity scratch is described in the present study. The present paper consists of the roadmap of finite-element scratch model development. The step by step evolution of the model from a simple 2D contact model to a 3D scratch model is explained in detail. Each step is validated either by analytical model or experimental results and the model has shown a considerable agreement.

## FINITE-ELEMENT MODEL DEVELOPMENT

### Roadmap

The present research aims at describing the development strategy of a finite-element model for scratch using ABAQUS (6.14). Hence, the path to achieve this goal was divided into four easy and simple steps of evolution listed below. The roadmap is laid out schematically in Table 1. These steps serve as building blocks aiding to learn and understand the process of model development, data extraction and analysis and the process of validation.

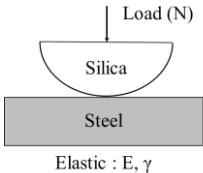
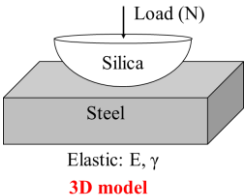
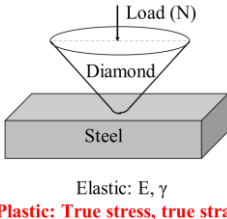
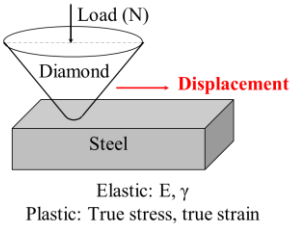
- i. 2D Hertzian line contact
- ii. 3D Hertzian point contact
- iii. 3D Indentation
- iv. 3D Scratch

Based on the type of problem we are trying to solve, two types of problem solving algorithms can be implemented in ABAQUS, namely, implicit and explicit. The fundamental difference in both the approaches is that in explicit scheme of analysis the values at time,  $t + \Delta t$  are calculated based entirely on time  $t$  whereas in the implicit scheme the value at  $t + \Delta t$  is obtained based on  $t$  and  $t + \Delta t$  which results in solving a set of non-linear equations (Chapra & Canale, 1988). Further details regarding these two schemes can be found in ABAQUS theory guide ("Abaqus documentation 6.14 ", 2014)

The first two models are static processes, as they do not require time dependent material response and the inertial effects were insignificant. Therefore, they are solved using the implicit scheme in ABAQUS/Standard. The third model of 3D indentation can be considered either as a static or a quasi-static process (inertial effects can be neglected but time-dependent material response is of interest). Thus, this model is solved using both implicit and explicit scheme by implementing ABAQUS/Standard and ABAQUS/Explicit respectively. This exercise helps not only to understand the nuances of the two approaches in detail, but also serves as a foundation for the development of the next step. The subsequent addition to the explicit 3D indentation model is to introduce the displacement of the indenter in order to achieve the scratch model.

The evolution of each stage of model development with respect to the type of process, model, etc., is summarized in Table 1. The first row describes the type of process and the solution scheme adopted to solve the model. The second row describes the type of model developed and the third row contains schematic representation of the models. The novelty of each stage is mentioned clearly in the figures. For example, the difference between the first two models is due to the dimensions, that is, the first model is a two-dimensional model whereas the second model was three-dimensional. Plasticity was introduced in the third model and displacement of the indenter was the uniqueness of the fourth model.

Table 1: Roadmap of scratch model development.

STATIC-IMPLICIT		QUASI-STATIC-EXPLICIT	
2D Hertzian line contact	3D Hertzian point contact	3D Indentation	3D Scratch
 <p style="font-size: small;">Elastic : E, <math>\gamma</math></p>	 <p style="font-size: small;">Elastic: E, <math>\gamma</math></p> <p style="color: red; font-weight: bold; font-size: small;">3D model</p>	 <p style="font-size: small;">Elastic: E, <math>\gamma</math></p> <p style="color: red; font-weight: bold; font-size: small;">Plastic: True stress, true strain</p>	 <p style="font-size: small;">Elastic: E, <math>\gamma</math></p> <p style="color: red; font-weight: bold; font-size: small;">Plastic: True stress, true strain</p>

### 2D Hertzian line contact model

The first step was to develop a simple two-dimensional finite-element model. The purpose of the two-dimensional model was to get acquainted with the process of model development, result extraction and analysis followed by verification of the model using analytical solutions. The model consisted of two deformable parts with semicircular ( $\Phi 1$  mm) and rectangular geometry (0.5 mm x 1 mm). The material properties listed in Table 2 were used to define the materials. The properties of silica and steel were assigned to the semicircular and rectangular parts respectively. In order to extract contact pressure from the model, plastic properties of the parts is not required. Therefore, only

the elastic properties of the materials of the materials were used. The parts were partitioned appropriately and the area of contact being the region of interest was meshed finer than the rest of the model. The finest element size was 1  $\mu\text{m}$ . A 4-node bilinear plane strain quadrilateral (CPE4) element type was used.

Table 2: Material properties of Silica and Steel

	Elastic modulus, GPa	Poisson's ratio
Silica	73	0.17
Steel	210	0.3

A frictionless, surface-to-surface contact was defined. The harder surface, silica, was defined as the master and the surface of the steel part was defined as the slave. A concentrated force was applied normal to the area of contact. Appropriate boundary condition of restricting the motions of the nodes on the side edges and the bottom of the specimen were imposed ( $U_1=U_2=U_3=0$ ). The semicircular part was also restricted to move in the X direction ( $U_1 = 0$ ). The von-Mises stresses (S) developed in the model are shown in Figure 1.

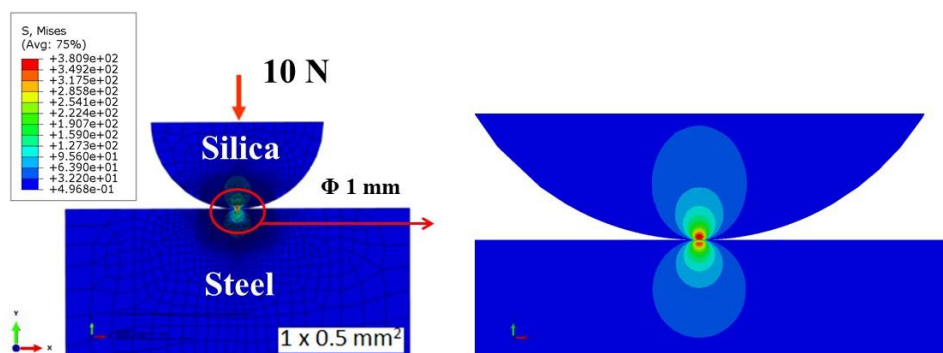


Figure 1: Two-dimensional Hertzian line contact model showing the von-Mises stress (S) distribution in the model

### 3D Hertzian point contact

The two-dimensional model developed in the previous step was further extended into a three-dimensional model. The three-dimensional model consists of two parts a hemisphere ( $\Phi 1\text{ mm}$ ) and a cube ( $0.5\text{ mm} \times 0.5\text{ mm} \times 0.5\text{ mm}$ ) as shown in Figure 2. The hemisphere was assigned the properties of silica whereas the cube was defined with the properties of steel. Since, contact pressure was being evaluated in this case too, only elastic properties were sufficient for material model definition. The region of interest being the point of contact had been finely meshed with an element size of 5  $\mu\text{m}$ . A similar surface contact, load and boundary conditions were implemented in the three-dimensional model as the two-dimensional model. The four side faces and the bottom of the specimen were bounded and the hemisphere was allowed only to move in the Y-direction. The contact stress distribution along the surface is shown in Figure 2 (b). The maximum contact pressure is 2.884 GPa.

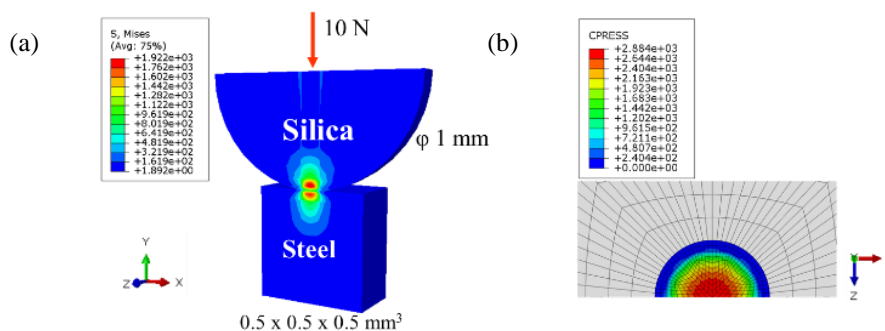


Figure 2: Three-dimensional Hertzian point contact model. (a) von-Mises stress (S) distribution in the model; (b) Contact pressure (CPRESS) distribution across the surface. The maximum contact pressure being 2.884 GPa.

### 3D indentation model

The three-dimensional indentation model simulates experimental microhardness indentation. The novelty of this model is the introduction of plasticity into the material definition of the specimen. Therefore, the specimen was defined as homogenous elasto-plastic deformable material. The elastic properties as shown in Table 2 were used whereas experimentally obtained true stress-true strain properties were used to define the plasticity of the steel specimen. The indenter was defined as analytically rigid cone of  $120^\circ$  included angle and a tip radius of 0.1 mm. A concentrated normal load of 25 N was applied on the indenter (see Figure 3). The increase in indentation depth with increase in applied load was plotted (see Figure 6(a)). The residual depth of indentation after elastic recovery was observed to be  $20.8 \mu\text{m}$ .

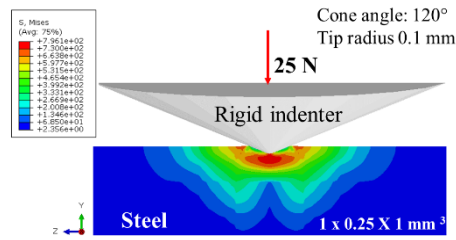


Figure 3: Three-dimensional indentation model involving a rigid cone with cone angle of  $120^\circ$  and a tip radius of 0.1 mm and an elasto-plastic deformable steel specimen (1 mm x 0.25 mm x 1 mm)

### 3D scratch model

The final step was to develop a finite-element model to simulate scratch. Scratch simulation involves the tangential movement of the indenter with respect to the specimen. In the present simulation the indenter is subjected to a displacement equal to the scratch length. The indenter geometry was similar to the previous indentation model. The specimen dimensions of the elasto-plastic deformable material were 3 mm x 0.5 mm x 1 mm (see Figure 4). The scratch length was 2.5 mm. Mean scratch depth is defined the average displacement of the nodes along -Y axis between the scratch length of 1 to 2 mm. The mean scratch depth obtained for different scratch loads is plotted in Figure 6(b).

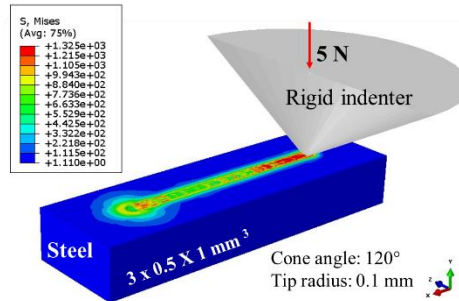


Figure 4: Scratch model involving a rigid conical indenter and an elasto-plastic deformable steel specimen.

## VALIDATION

The finite-element models developed were verified using analytical equations or validated using experimental results at each step. The verification of two-dimensional Hertzian line contact model was done using analytical equations of Hertz contact model (Bhushan, 2013). The analytical equations to calculate the effective contact radius ( $R^*$ ) and effective Young's modulus ( $E^*$ ) are given in equation (1) and (2) respectively.  $R_1$  and  $R_2$  are the radii,  $E_1$  and  $E_2$  are the elastic moduli and  $\nu_1$  and  $\nu_2$  are Poisson's ratio of the two surfaces in contact.  $W$  is the normal load applied. The maximum contact pressure  $p_{max}$  is calculated using equation (3) for Hertzian line contact.

The comparison between the results obtained from the analytical solution and simulation is shown in Figure 5 (a). The maximum contact pressure was 600.81 and 598.17 MPa from analytical and simulated results respectively with an error of 0.4 %. Similarly, the three-dimensional Hertzian point contact model was verified using equations (1), (2) and (4). The equation of the maximum contact pressures varies in this case due to the change in the contact

configuration. The maximum contact pressure obtained using analytical and simulations were 2.92 and 2.88 GPa with an error of 1.37 % as shown in Figure 5 (b).





(a)	Maximum contact pressure, MPa		(b)	Maximum contact pressure, GPa	
Analytical	600.81		Analytical	2.92	
Simulated	598.17		Simulated	2.88	
	<b>Error 0.4%</b>			<b>Error 1.37%</b>	

Figure 5: Comparison of analytical and simulated results; (a) Hertzian line contact (b) Hertzian point contact

The indentation model was validated indirectly using experimental results. A two-dimensional indentation model which was validated against experimental results was already available. Therefore, this two-dimensional model was used to validate the 3D model developed. The increase in force with increase in scratch depth for both the

$$\frac{1}{R^*} = \frac{1}{R_1} + \frac{1}{R_2} \quad (1)$$

$$\frac{1}{E^*} = \frac{1 - \nu_1^2}{E_1} + \frac{1 - \nu_2^2}{E_2} \quad (2)$$

$$\text{Hertzian line contact, } p_{max} = \left( \frac{WE^*}{\pi R^*} \right)^{1/2} \quad (3)$$

$$\text{Hertzian point contact, } p_{max} = \left( \frac{6WE^{*2}}{\pi^3 R^{*2}} \right)^{1/3} \quad (4)$$

two-dimensional and three-dimensional indentation models is plotted in Figure 6 (a). The difference between the residual depth of the 2D and 3D model is 1 %. The scratch model developed were validated using experimental results as shown in Figure 6 (b). The experiments were carried out using CSM scratch tester and details of the test procedure and equipment can be found elsewhere (Xu, van der Zwaag, & Xu, 2015). Mean scratch depth at 6 different scratch loads is plotted for simulated and experimental results and it can be seen that the simulated results are in good agreement with experimental results.

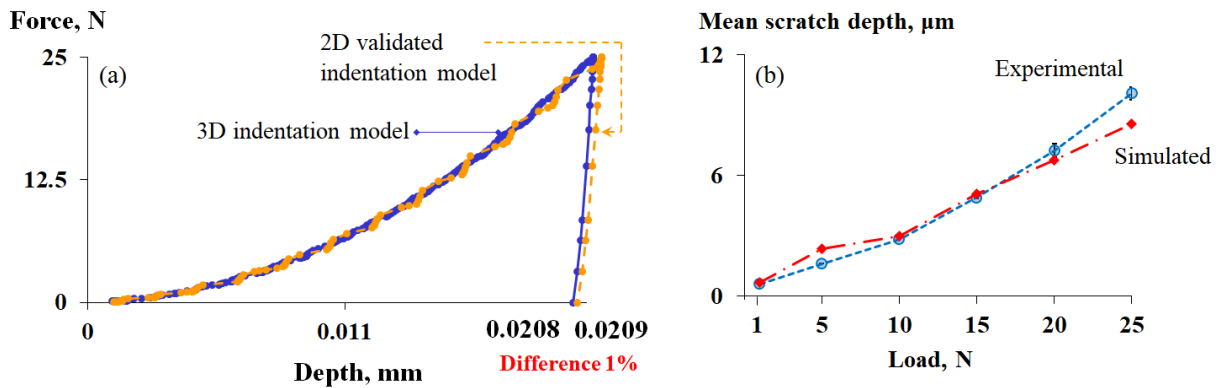


Figure 6: Validation of indentation and scratch models; (a) Comparison of force-depth curve of the 3D indentation model developed and 2D validated model. The residual depth is showing a difference of 1 %. (b) Comparison of experimental and simulated scratch results; Increase in the mean scratch depth with load is plotted. Simulated results are in good agreement with experiments.

## CONCLUSIONS

The goal of finite-element model development for scratch has been successfully achieved with the help of the roadmap laid out. At each stage of evolution, the model has been successfully validated. The contact models both two-dimensional and three-dimensional are verified by analytical solutions. The indentation model also shows good agreement with a previously validated two-dimensional model. The results from the scratch tests and scratch simulations are in good agreement with each other. Future work involves understanding the effects of various parameters such as indenter geometry, sliding velocity, etc.

## ACKNOWLEDGEMENTS

I would like to express my deepest gratitude to Dr. ir. Tonyan Yue and Mrs. Kyvia Pereira for their valuable advice and support during the initial stages of model development. I would like to thank Dr. Ir. Xiaojun Xu for conducting the validation experiments for scratch tests at NOVAM group, TU Delft. The research has been carried out in the frame work of MaDurOS program financed by SIM and VLAIO-Flanders.

## REFERENCES

- Abaqus documentation 6.14 (2014). from Dassault Systems, SIMULIA Corp.
- ASTM. (1987). Annual book of standards *ASTM G40, Standard terminology relating to wear and erosion* (pp. 243-250). West Conshohocken.
- Bhushan, B. (2013). *Introduction to tribology*: John Wiley & Sons.
- Chapra, S. C., & Canale, R. P. (1988). Numerical methods for engineers: McGraw-Hill New York.
- Elwasli, F., Zenzemi, F., Mkaddem, A., Mzali, S., & Mezlini, S. (2015). A 3D multi-scratch test model for characterizing material removal regimes in 5083-Al alloy. *Materials & Design*, 87, 352-362.
- Gerbig, D., Srivastava, A., Osovski, S., Hector, L. G., & Bower, A. (2017). Analysis and design of dual-phase steel microstructure for enhanced ductile fracture resistance. *International Journal of Fracture*, 1-24.
- Jankowiak, T., Rusinek, A., Kpenyigba, K. M., & Pesci, R. (2014). Ballistic behavior of steel sheet subjected to impact and perforation. *Steel and Composite Structures*, 16(6), 595-609. doi:10.12989/scs.2014.16.6.595
- Li, J., & Beres, W. (2006). Three-dimensional finite element modelling of the scratch test for a TiN coated titanium alloy substrate. *Wear*, 260(11-12), 1232-1242. doi:http://dx.doi.org/10.1016/j.wear.2005.08.008
- Mason, B. H., & Warren, J. (2017). Finite Element Simulation of Three Full-Scale Crash Tests for Cessna 172 Aircraft *58th AIAA/ASCE/AHS/ASC Structures, Structural Dynamics, and Materials Conference: American Institute of Aeronautics and Astronautics*.
- Ni, J., & Abdel Wahab, M. (2017). A numerical kinematic model of welding process for low carbon steels. *Computers & Structures*, 186, 35-49. doi:http://dx.doi.org/10.1016/j.compstruc.2017.03.009
- Subhash, G., & Zhang, W. (2002). Investigation of the overall friction coefficient in single-pass scratch test. *Wear*, 252(1-2), 123-134. doi:http://dx.doi.org/10.1016/S0043-1648(01)00852-3
- Tobi, A. M., Sun, W., & Shipway, P. (2017). Investigation on the plasticity accumulation of Ti-6Al-4V fretting wear by decoupling the effects of wear and surface profile in finite element modelling. *Tribology International*, 113, 448-459.
- Xu, X., van der Zwaag, S., & Xu, W. (2015). A novel multi-pass dual-indenter scratch test to unravel abrasion damage formation in construction steels. *Wear*, 322-323, 51-60. doi:http://dx.doi.org/10.1016/j.wear.2014.10.011
- Yue, T., & Wahab, M. A. (2017). Finite element analysis of fretting wear under variable coefficient of friction and different contact regimes. *Tribology International*, 107, 274-282.
- Zmitrowicz, A. (2006). Wear patterns and laws of wear - A review. *Journal of Theoretical and Applied Mechanics*, 44(2), 219.